https://doi.org/10.1142/9789811278952_0007

Chapter 7

RF Systems

R. Calaga[a], P. Baudrenghien[a], G. Burt[b], O. Capatina[c], E. Jensen[d], E. Montesinos[a] and A. Ratti[e]

[a]*CERN, SY Department, Genève 23, CH-1211, Switzerland*

[b]*University of Lancaster, Lancaster LA1 AYW, UK*

[c]*CERN, EN Department, Genève 23, CH-1211, Switzerland*

[d]*CERN, EP Department, Genève 23, CH-1211, Switzerland*

[e]*SLAC, Palo Alto, California, CA 94025, USA*

The HL-LHC beams are injected, accelerated to and stored at their nominal energy of 7 TeV by the existing 400 MHz superconducting RF system of the LHC. A new superconducting RF system consisting of eight cavities per beam for transverse deflection (aka crab cavities) of the bunches will be used to compensate the geometric loss in luminosity due to the non-zero crossing angle and the extreme focusing of the bunches in the HL-LHC.

1. HL-LHC RF Systems

1.1. *Accelerating RF*

In the LHC, a "half-detuning" scheme was originally proposed and implemented to provide a constant voltage (amplitude and phase) while keeping the klystron power constant over one turn. The klystron drive phase is flipped between and beam and no-beam segments with the loaded Q optimized for minimum power.[4] Due to doubling of the beam currents in the HL-LHC, an optimal detuning scheme (aka "full-detuning") is required to cope with the transient beam loading effects during the energy ramp and collisions.[1,2] A modulation of the klystron and cavity phase make the phase of bunches with

respect to the RF clock to progressively slip along the bunch train, but then recover during the long abort gap. With this scheme the klystron power is independent of the beam current and maintained constant over one full turn at the expense of bunch-to-bunch phase modulation. This scheme was experimentally tested in 2016 and has been operational since then in the LHC during the acceleration ramp and flat-top.[3] During injection of the HL-LHC beams from the SPS in to the LHC however, the original half-detuning scheme to strictly preserve the bunch-to-bunch spacing is a pre-requisite.

1.2. *Crab Crossing*

For higher luminosity operation, proton beams are squeezed to very small β^* at IP1 and IP5 (well below the nominal 55 cm). Controlling the effect of the large number of parasitic collisions requires a non-zero crossing angle. A non-zero crossing angle in combination with small β^* however implies a geometric reduction of the luminosity $R_\phi = (1 + \phi^2)^{-1/2}$ due to non-perfect overlap of the colliding bunches. This effect is illustrated in Figure 1 and compared to crab crossing scheme where the head and the tail of the bunches transported along different orbits to maximize the overlap at the interaction point.

Fig. 1. Bunches colliding with a crossing angle without crab crossing (left); with the crab crossing (right).

The HL-LHC upgrade will use deflecting (or crab) cavities to compensate for geometric luminosity loss. Two schemes were considered for crab crossing in the HL-LHC, the global scheme and the local scheme. The global scheme would require a single crab cavity system per beam, installed e.g. near point 4, where presently all LHC RF systems are installed with an appropriate phase advance between the crab cavities and the IPs. The transverse kick introduced by this cavity, different for the head and the tail of each bunch, is equivalent to a closed orbit distortion, i.e. head and tail would follow their individual closed

orbit around the ring, their tilt wobbling around the unperturbed closed orbit of the bunch centre. It is clear that this scheme introduces severe constraints on the betatron phase advance between the location of the crab cavities and the IPs. It is also inconsistent with the different crossing angles implemented in IP1 (horizontal crossing) and IP5 (vertical crossing). Furthermore, the collimator settings would have to allow for the wobbling bunches.

The local scheme on the other hand introduces a localized perturbation upstream of the IP where crabbing is required and compensates for it downstream, such that through the rest of the ring the bunches remain unperturbed. This scheme requires up to 4 pairs of cavities per beam and per IP for a full compensation of the HL-LHC crossing angle. So up to 32 cavities are required if only the high luminosity regions (IP1, IP5) are considered. This scheme does not have the optics constraints of the global scheme between the two IPs and allows for the different crossing planes in IP1 and IP5. On the other hand it requires more cavities and in particular cavities that are compact enough for the nominal beam pipe distance of 194 mm. As a result of an intense R&D effort within the HL-LHC collaboration, three novel compact cavity geometries were successfully developed and tested for the HL-LHC.

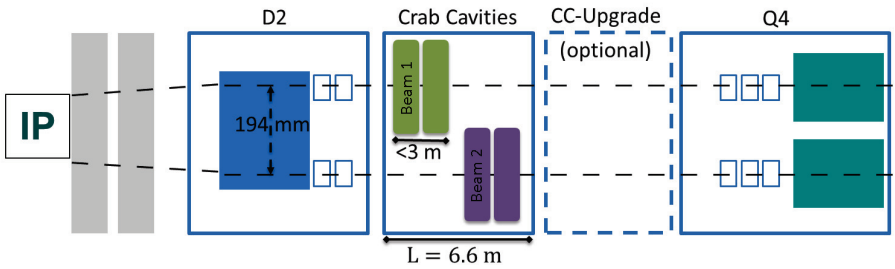

Fig. 2. Schematic layout of the crab cavities in the LHC Point 1 and 5 w.r.t the interaction point.

A local scheme with crab cavity pairs across the IPs is therefore established as the baseline using compact crab cavities at 400 MHz (see Figure 2). Design of the cavities, the cryomodules and the RF system is described in the following sections. A validation of the crab crossing with protons in the Super Proton Synchrotron (SPS) as the first phase towards the implementation in HL-LHC is also described.

1.3. *Transverse Damper*

The LHC requires a transverse feedback to damp injection oscillations and provide stability for impedance-driven transverse instabilities, thus guaranteeing preservation of beam intensity and emittance. The existing coupled bunch feedback system (ADT), installed in Point 4 of the LHC, was fully commissioned in 2010.[9] It dampens transverse instabilities within a bandwidth of 20 MHz, correcting the oscillations of the centre of gravity of the individual bunches about their orbit. Beyond 20 MHz, the kicker and ADT power amplifier system cannot be used. For the HL-LHC, studies on a larger bandwidth transverse damper were performed in view of the high bunch intensity, but the present ADT system was deemed sufficient for HL-LHC operation.

2. Crab Crossing and Technology Choice

The HL-LHC parameters for a 7 TeV proton beam calls for superconducting crab cavities at a frequency of 400.79 MHz. The frequency choice is primarily driven by the long proton bunches, but it is also convenient to use the same frequency as the accelerating RF system. A total crab cavity voltage of approximately 12 MV is required at 400.79 MHz per IP side per beam to perform the complete bunch rotation. Assuming a maximum voltage of 3.4 MV per cavity, four cavities per side per beam per collision point, i.e. a total of 32 cavities are needed for full compensation. However, only half the system, 16 cavities, are to be installed after the re-baselining in 2016, allowing a partial compensation.[8] Two cavities are assembled into a cryomodule as a fundamental unit to provide an integrated kick voltage of 6.8 MV.

2.1. *Physical Constraints*

Seen from the IP, the cavities are placed outside the recombination dipole D2, where the beams are completely separated and in their individual beam pipes spaced by 194 mm, and the β-functions in the crossing plane are sufficiently large to minimize the required voltage. Due to remaining optical constraints, the ideal betatron phase advance of $\pi/2$ between IP and crab cavities may not be realized exactly; the orbit bump from the crossing angle is closed prior to the entry into the crab cavities to minimize beam loading effects with trajectory

offsets. The tightest constraint results from narrow beam pipe spacing in the transverse plane. Measuring from the electric centre of the cavity (where the integral $\int_{-\infty}^{\infty} E_z e^{j\frac{\omega}{c}z} dz$ of the operating mode vanishes), the beam pipe at both ends of the cavity must leave a disk of radius 42 mm clear; this will allow the transverse alignment of the cavity without reducing the aperture for the beam. To allow passage of the 2nd beam pipe (distance centre to centre 194 mm) it is required that the cavity transverse size does not extend beyond 145 mm from the same electric centre. Since both vertical and horizontal crossing are used, these tight constraints have to be respected in the crossing plane and the plane orthogonal to it. In the longitudinal plane, the constraints are primarily dictated by the proximity to the neighbouring elements, namely the D2 recombination dipole and the Q4 matching section quadrupole. A total of 13.3 m is reserved for two pairs of four cavities per IP.[5]

2.2. *RF Cavities*

In order to sustain the surface fields at a kick voltage of 3.4 MV per cavity for the HL-LHC in continuous wave (CW), superconducting technology using high purity bulk Niobium is essential; space restrictions, voltage requirements, and impedance considerations strongly rule out a normal conducting option. Transverse space restrictions led to the concept of 'compact' cavities.

2.2.1. *Cavity Geometry*

As a result of an intense R&D within the FP7 HiLumi LHC, EuCARD and LARP programs and with other external collaborators, three compact designs at 400 MHz emerged as potential candidates.[6,7] The three proposed designs are at least four times smaller in the plane of crossing compared to a conventional elliptical cavity with a ratio of the kick gradient to the peak surface fields lower by a factor of 2 or better. After validation of the superconducting prototypes within the collaborations, two designs were retained towards their implementation in HL-LHC for vertical and horizontal kick, the Double Quarter Wave (DQW) and the RF Dipole (RFD). The final mechanical design of the cavities including all external interfaces is shown in Figure 3.

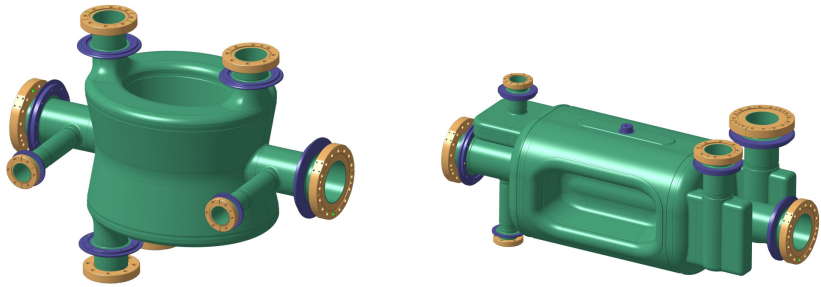

Fig. 3. Schematic view of the cavity with interfaces (left) DQW; (right) RFD.

Table 1. RF parameters for the DQW and RFD cavities.

Quantity	Unit	Value
Frequency	MHz	400.79
Bunch length	ns	1.0-1.2 (4 σ)
Maximum cavity radius	mm	$\leq$ 145
Nominal kick voltage	MV	3.4
R/Q (linac convention)	Ω	430
Q_0		$\geq 10^{10}$
Q_{ext} (fixed coupling)		5×10^5
RF power	kW-CW	40 (80 peak, 1 ms)
LLRF loop delay	μs	≈ 1
Cavity detuning (if parked, optional)	kHz	≈ 1.0

2.2.2. *RF Multipoles*

The main deflecting field of the chosen crab cavity geometries contain higher order components of the main deflecting field dependence due to the lack of azimuthal symmetry. Due to the placement of the cavities at high beta-function locations, the higher order components of the main deflecting mode can affect long-term particle stability. RF multipole components b_n of the RF deflecting field can be approximated and hence expressed in a similar fashion to magnets:[10]

$$b_n = \int_0^L \frac{1}{qc} F_\perp^n dz = \frac{jn}{\omega} \int_0^L E_{acc}^n dz \quad [\mathrm{T\,m^{2-n}}] \tag{1}$$

Due to symmetries inherent to each design, only odd multipoles have a non-zero component. However, due to fabrication errors and ancillary components,

the first and most important even multipole, b_2, is non-zero. Specifications from beam dynamics indicate that this value be smaller than 10 units leading to a tune shift of the order of $\Delta Q \approx 10^{-4}$. The first systematic multipole is the sextupolar component, b_3. Long-term simulations with the optical functions of the HL-LHC indicate that the b_3 component should be limited to approximately $1500 \pm 10\%$ units, which results in an acceptable degradation of the dynamic aperture below 1 σ for orbit offsets of 1.5 mm.[11] Both the DQW and the RFD designs are below the specified tolerance for b_3. It is expected that they can be controlled to smaller values than the neighbouring D2 dipole magnet. For $n \geq 4$, assuming a very approximate scaling of the additional kick from an orbit offset via b_n, the b_n must be kept below $\propto O(10^n)$. More precise specifications for higher order terms require long-term tracking simulations.

2.3. *Dressed Cavities*

The ensemble of the helium tank, cold magnetic shield, fundamental power coupler, HOM couplers and the frequency tuning system is referred to as dressed cavity and described below.

2.3.1. *Helium Tank*

The helium tank will contain saturated superfluid helium at 2 K, cooling the cavity and allowing the extraction of the heat dissipated in the cavity and adjacent cold components. The titanium grade 2 was chosen as the optimum material for the helium tank, allowing for rigid connection of cavity ports to it. The helium tank has a structural role, and its rigid connection to the cavity ports ensures optimum boundary conditions for the cavity during mechanical loading, in particular during maximum pressure loading and tuning. Therefore, a novel concept using a bolted design with additional leak proof welds to minimize the stress on the cavity during the assembly of the Helium vessel Figure 4. Due to the large apertures in the external magnetic shield for couplers and beam pipes, a single layer is not sufficient to completely shield the earth's magnetic field to the required level ($\leq 1\,\mu$T) with sufficient safety margin. A second cold shield (in purple) is integrated inside the helium vessel (light blue), as presented in Figure 4. The internal shield is 1 mm thick and will be made from Aperam Cryophy® to operated at 2 K.

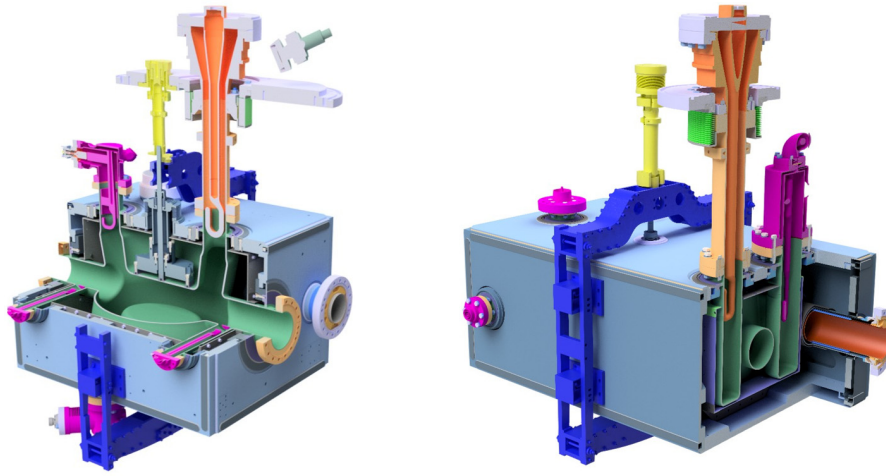

Fig. 4. Left: Sectional view of the DQW cavity inside its helium tank with the power coupler (top right, orange), HOM coupler (left, top and bottom, violet), and tuner (centre, top, and bottom). Right: Schematic sectional view of the RFD cavity inside its helium tank with the power coupler (orange) and HOM couplers (violet).

2.3.2. *RF Power Coupler*

In deflecting cavities operated in the crabbing mode, kick voltage and beam current are in quadrature ($\phi_s = 0$, synchrotron convention). The longitudinal impedance of the operating crabbing mode vanishes on axis, i.e. there is no beam loading for a centred beam; the RF generator does not exchange energy with the beam. The RF power required to maintain the required cavity voltage thus only depends on the cavity wall losses and remains small for a superconducting cavity with large Q_0 and Q_L. The input coupling and thus Q_L should be chosen to just allow sufficient bandwidth for unavoidable frequency transients due to external perturbations.

The situation is different for a beam circulating at an offset Δx. The beam-induced voltage due to an orbit offset is given by

$$\Delta V = I_b \cdot \frac{R}{Q_0} \cdot Q_L \cdot \Delta x \tag{2}$$

where I_b is the average beam current, $R_T = R/Q_0 \cdot Q_L$ is the transverse shunt impedance in Ω/m. With the Q_L resulting from the bandwidth requirement

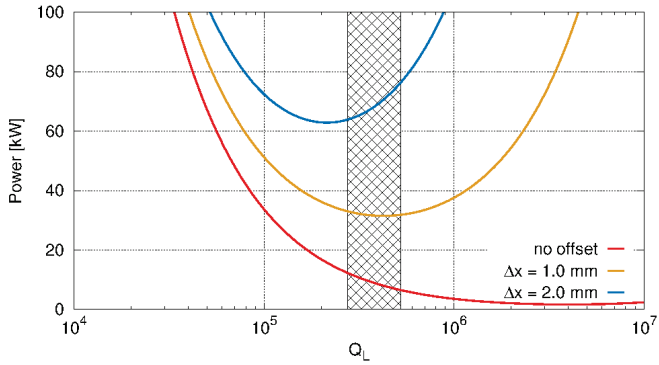

Fig. 5. Forward power vs. cavity Q_L for centred (red), 1 mm offset (green), and 2 mm offset (blue) beams. Assumed $R_T Q = 430\,\Omega$, 3.4 MV RF, 1.1 A DC beam current.

discussed above, sufficient RF power is required to compensate for the resulting beam loading caused by unavoidable orbit offsets. Figure 5 shows the required forward power as a function of Q_L for a beam that is centred (red), off-centred by 1 mm (green) and 2 mm (blue). The RF power is limited to 40 kW-CW with a capability of provide 80 kW peak for approximately 1 ms to cope with transients. Therefore, the orbit must be kept within ±0.5 mm at top energy of the LHC; further 0.5 mm is assumed for intra-cavity alignment and mechanical tolerances. At injection and ramp, the operating voltage is kept at 10-15% of the nominal voltage. Therefore, beam offset tolerance are much relaxed with the available 40 kW-CW RF power.

The crab cavity power coupler will use a single coaxial disk-type window to separate the cavity vacuum and the atmospheric pressure. The antenna shape uses a "hook" design to principally couple magnetically to the deflecting mode. The exact hook shape is specific to each cavity type as the coupling mechanisms on the cavity are not identical between DQW and RFD cavities. The ambient pressure side of the coupler will be air-cooled while the antenna itself will be water-cooled. The waveguide design includes the possibility of DC polarization in order to suppress multipacting.

2.3.3. *Higher Order Mode Couplers*

On resonance, the large impedance of the fundamental deflecting (dipole) mode is cancelled between the positive and negative sideband frequencies,

which are symmetric around ω_{RF}. The active feedback will reduce the growth rates by a large factor.

For higher order modes (HOMs), both narrow-band and broadband impedance should be minimized during the entire machine cycle as the LHC will accelerate and store beams of currents exceeding 1.1 A (DC). The tolerable longitudinal impedance has approximately a quadratic behaviour vs. f in the region of interest with its minimum between 300 and 600 MHz. The total maximum allowed impedance from each HOM, summing over all cavities in one beam, assuming that the HOM fall exactly on a beam harmonic, is specified to be $\leq 200\,\mathrm{k}\Omega$. The same limit was imposed for higher frequencies. Modes with frequencies above 2 GHz are expected to be Landau-damped due to natural frequency spread and synchrotron oscillations.

In the transverse plane, the impedance threshold is set by the bunch-by-bunch feedback system with a damping time of $\tau_D = 5\,\mathrm{ms}$. Four effective cavities per beam are assumed due to the two different cavity types with different HOM spectra. The single bunch studies show that integrated R_T/Q

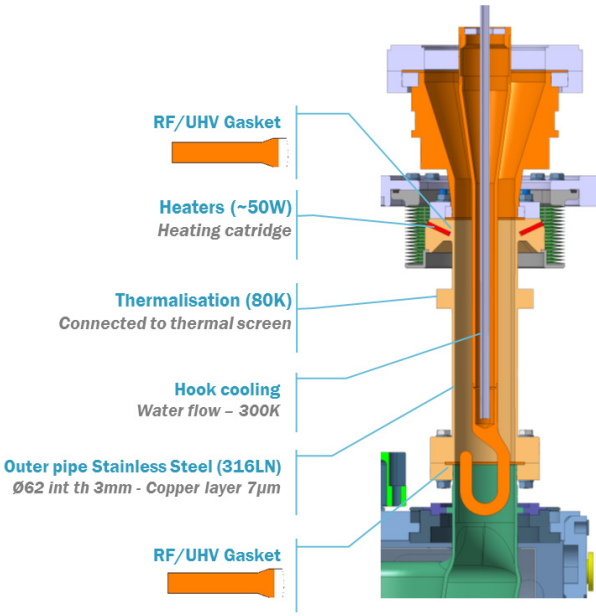

Fig. 6. Fundamental power coupler for the DQW cavity. Similar concept is adopted for the RFD with its own coupling hook.

over the frequency for all the HOMs per cavity should be suppressed to below 4 kΩ/m (without accounting for β-function) from stability considerations.[5] From multi-bunch considerations and assuming the pessimistic case that the HOM frequency coincides with the beam harmonic, the maximum total transverse impedance in each plane is set to be 1 MΩ/m.[5] Analogous to the longitudinal modes, frequencies above 2 GHz are expected to be Landau-damped due to natural frequency spread, chromaticity, and Landau octupoles. Due to the very tight impedance thresholds, the distribution of HOM frequencies as mentioned above due to manufacturing errors can help relax the tolerances.

Several HOM coupler designs were developed and optimized to provide a high transmission over a large bandwidth of 0.5 - 2 GHz while suppressing the coupling to the fundamental mode. Figure 7 shows the final HOM geometries for the DQW and the RFD respectively. The DQW uses three on-cell HOM couplers with hook-type magnetic coupling to reach the impedance specifications. An additional mushroom-type antenna placed on the cavity beam pipe is required to damp certain high frequency modes confined near the beam pipe region. The RFD uses two hook-type HOM couplers, one for each transverse plane. Both couplers are mounted on dedicated waveguide stubs which act to limit the fundamental mode field near the HOM coupler antenna. The horizontal HOM coupler requires a notch filter at 400 MHz to suppress the coupling to the deflecting mode while the vertical HOM coupler relies on the orientation of the waveguide stub parallel to the deflecting field which acts as a natural filter. Simulations show that the HOM coupler must have a superconductive surface due to the high fields of the fundamental mode and

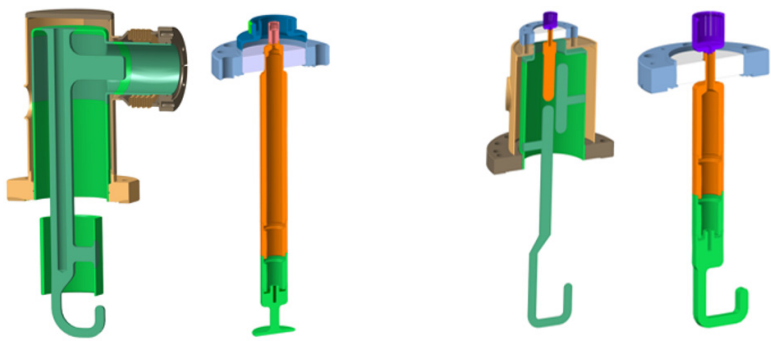

Fig. 7. HOM couplers for the DQW (left) and the RFD (right).

limit the heat load to the 2 K Helium bath for both cavities. Active cooling for the in-cell HOM couplers in the DQW cavity to minimize thermal gradients of the superconductive surface is used (see Figure 7).

The beam power deposited in the longitudinal HOMs can become significant when the frequencies coincide with bunch harmonics. The HOM couplers were dimensioned to cope with maximum of 1 kW average power to be able to cope with HL-LHC type beams.

2.3.4. *Frequency Tuning*

The final resonance frequency of the cavity will depend on a number of fabrication and handling steps and cool-down. A 'slow' mechanical tuning system is required to compensate for the uncertainties of the above steps by altering the cavity shape – this will dominate the tuner requirement. At 2 K it must be possible to tune the cavity to $f_{res} = f_{operation} \pm \Delta f_{LFD}$, where Δf_{LFD} denotes Lorentz force detuning occurring during cavity filling. The operational tuning range required in the LHC is approximately a few kHz. A large tuning range ($\approx \pm 200$ kHz) is specified to cope with frequency variations from cool-down and other mechanical deformations. However, the resolution of the tuner should allow at least ten steps inside the cavity bandwidth (≈ 800 Hz); backlash and hysteresis must be small.

The tuning system is similar for both cavities (DQW and RFD). It consists of an actuation system that is placed outside the cryomodule, and operated at room temperature and at atmospheric pressure, which makes it accessible and thus maintainable.[18] The actuation system consists of a high resolution stepper motor (1.8 deg/step), a harmonic gearbox (100:1 ratio), a roller screw, and linear guide bearings. The estimated mechanical resolution of the tuning system at the connection to the cavity is estimated to be in the order of 10 nm or less, which is equivalent to a few tens of Hz for both cavities, allowing for at least 10 micro-steps inside the cavity RF frequency bandwidth. The details of the prototype actuation system are shown in Figure 8. Since the cavity will be operated in CW mode and frequency variations are expected to be small, fast active tuning is not needed in the final design. The cryostat vacuum exerts a non-negligible force on the tuner mechanism, as it remains floating with respect to the vacuum vessel. A pressure compensation feature is added to minimize this force.

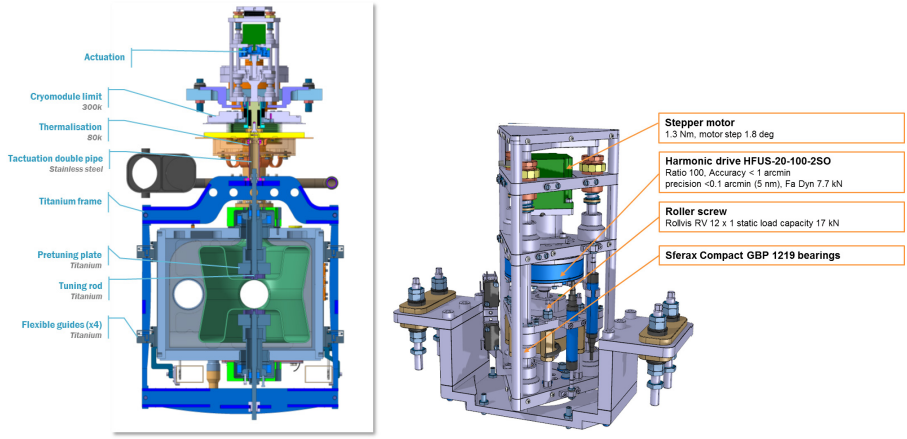

Fig. 8. Left: Cross-sectional view of the tuning system for the DQW cavity. Right: Actuation system of the prototype tuning system for DQW and RFD cavities.

2.4. *Cryomodule*

Machine architecture and integration studies for the LHC led to the choice of housing two individual cavities in one stand-alone cryomodule, individually connected to a cryogenic distribution line cryostat running in parallel with the main line. A total of six cold-to-warm transitions for the beam tube and four connections to the cryogenic distribution line are required for each cryomodule (Figure 9). This includes the adjacent beam pipe and related transitions which pass through the Helium jacket of the cavities. The combined static

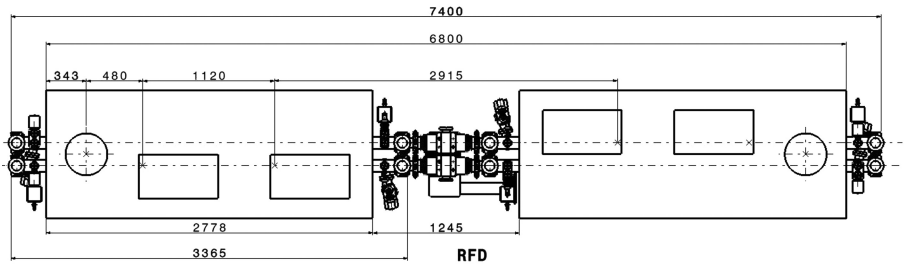

Fig. 9. Cryomodule layout for one side of the interaction region in the LHC for the RFD cryomodule. The layout of the adjacent beam pipe with its own cold-to-warm transitions are not shown.[19,20]

and dynamic cryogenic heat load at 2 K for the two cavities at operating nominal field is expected to be ≤ 50 W.[26] The exact length of the cryomodule depends on the cavity type and, for the longest cavity, results in a total of 7.4 m for two cryomodules (6.9 m for two cryomodules DQW) per side of the LHC interaction region for both beams including gate valves from the interconnection plane (see Figure 9). For each two-cavity module, two gate valves outside the cryomodule vacuum and corresponding vacuum equipment for pumping and monitoring outside at ambient temperature are foreseen.

The vacuum vessel is designed in two main parts – a lower vacuum tank and a top plate. It uses a top-down assembly procedure for the cavity string inside the vessel. This allows the possibility of cavity alignment with optical devices (laser trackers, for example) while making fine adjustments through the adjustable supports before closing the cryomodule. The cavity supporting concept uses the external conductor of the RF coupler as the main mechanical support of the dressed cavities. Two additional supporting points using flexural blades are used to keep cavity alignment stability within requirements. In the RFD cavity, the power coupler is transversely offset from the cavity axis, which requires additional vertical support. The complete cavity string is loaded into the vacuum vessel from the top, with plug valves fitted and closing end-plates integrated in the cavity string. This allows the closure of the beam vacuum in the clean-room environment to minimize contamination of the superconductive surfaces. All external connections except the beam pipes are on the top of the cryomodule. This allows easy access to the cavities and ancillaries. The designs for both cavity variants are kept as similar as possible.

2.5. *Cavity Alignment*

Successful operation of the RF cavities depends on their correct position. The transverse and longitudinal alignment tolerances are described in the LHC performance requirements:[4]

- Cavity rotation in the X-Y plane ("roll", Rz, Figure 10): it is required that this rotation has to be $< 0.3° = 5.2$ mrad ($3\,\sigma$) per cavity;
- Cavity "yaw" (RY) and "pitch" (RX) with respect to the cryostat axis should be $< 0.057° = 1$ mrad ($3\,\sigma$), Figure 10;
- Transverse displacement of cavities w.r.t each other inside a cryomodule: intra-cavity alignment in the transverse plane with respect to

the cryostat axis should not exceed the 0.5 mm (3 σ) tolerance set by beam loading and multipolar specifications.

The orientation and position of the cavity inside the cryomodule is adjusted by means of a plate rigidly connected to the dressed cavity in 3 supporting points. The rigid connection between the cavity and the alignment plate is obtained by means of the fundamental power coupler (FPC) and a set of additional blade type flexural supports.

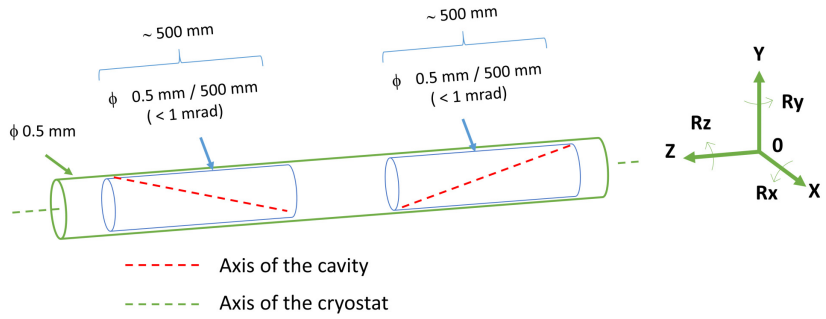

Fig. 10. Crab cavity alignment tolerances inside a two-cavity cryomodule.

The position of each cavity inside the cryomodule is measured by the frequency scanning interferometry (FSI) system.[16] The FSI system offers absolute interferometric distance measurement capability at sub-micron level at cold operating conditions and during the cavity cool down process. Only passive components (mirror, collimator, fibres) are needed at the cavity flange measurement points, which makes the application suitable for a high radiation level of operation. The FSI unit consists of a reference interferometer and a measurement interferometer that use tuneable lasers (from 1410 to 1510 nm). An additional second laser tuned in the direction opposite to the reference laser is required to correct the errors arising from drifts and to account for internal frequency and phase changes from the laser itself. The gas cell ensures stability of the reference interferometer. Each cavity features several FSI heads and several lengths between the FSI system heads and the reflective targets are measured in order to determine the position of the dressed cavities. An improvement from the experience gained from the SPS beam tests using multiple targets for added reliability and robust targets is under study for the eventual use in HL-LHC.

3. RF System and Controls

An independent powering system using SPS-type IOTs, modified to operate at 400 MHz, delivering 40 kW in CW and 80 kW peak is the current baseline for RF power. However, recent advances in solid-state technology allowed pursuing the study of an Solid State Power Amplifier [SSPA] based system in parallel to potentially replace the IOTs and to provide a flexible platform.

3.1. *RF Power*

The IOTs provide adequate power overhead in a compact footprint. This scheme would also allow for fast and independent control of the cavity set point voltage and phase to ensure accurate control of the closed orbit and the crossing angle in the multi-cavity scheme. Most importantly, fast control of the cavity fields will minimize the risk to the LHC during an abrupt failure of one of the cavities, ensuring machine protection before the beams can be safely extracted. For such fast and active feedback, a short overall loop delay between the RF system and the cavity is required. The overall architecture and approximate volume of the RF infrastructure is shown schematically in Figure 11, the circulators (brown) are placed in an RF gallery placed directly above the

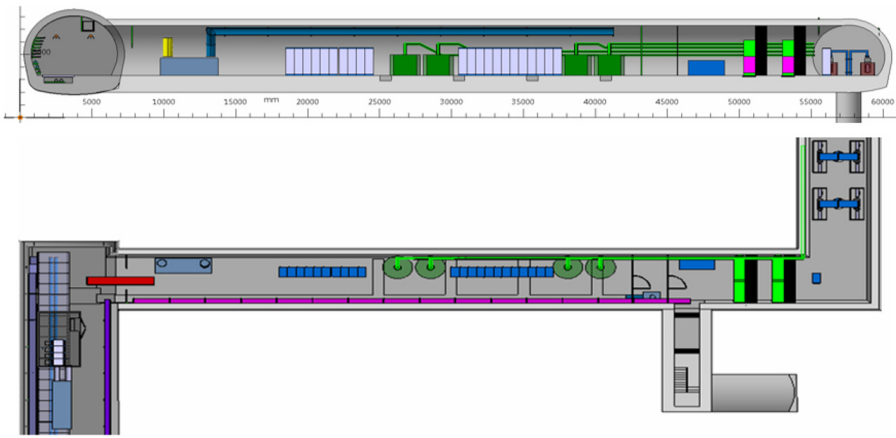

Fig. 11. Schematic of the RF system layout (four per IP side) in the underground cavern above the LHC tunnel lateral view (top); and top view (bottom). The amplifiers and transmission lines are shown in green routed torwards the tunnel located towards the right.

LHC tunnel with 1 m diameter vertical cores connecting the RF power lines. The circulator-to-cavity transmission lines will be WR2300 waveguide (blue) whilst amplifier-to-circulator transmission lines will be coaxial (green). The RF gallery is then connected to the main service gallery via a perpendicular tunnel, which is used to host power amplifiers and LLRF and also used for passage. Both the high power and the low level control systems are placed in the nearby underground gallery (UA) with access during beam operation.

3.2. *RF Feedback and Controls*

Limitations from the round-turn loop delay for the RF signal for cavity control should be taken into account for the fast feedback to cope with effects from fast RF failures. The amplifier driven by a feedback system feeds a compensating current to cancel the beam current. The cavity impedance is then effectively reduced by the feedback gain. Therefore, the limiting factor in the RF chain is the round-turn-loop delay. Therefore, a short distance between the cavity and the power amplifiers is preferred.[15] Above a certain feedback gain, the loop delay will drive the feedback into electrical oscillations. The minimum effective impedance is

$$R_{min} \approx \frac{R}{Q_0}\omega_0 T, \tag{3}$$

where ω_0 is the RF frequency, R/Q the classic cavity parameter and T the group delay of the feedback loop. Therefore, a radiation free cavern close to the crab cavity location in the LHC tunnel is required to keep the RF feedback delay to less than about 1.5 μs. This allows a significant reduction of the cavity impedance seen by the beam.

A rapid and unforeseen change of the field in one cavity (see Section 5.4) should trigger the LHC Beam Dump System (LBDS) to extract the beam in a minimum time of three turns (270 μs). The RF controls should minimize the effect on the beam within the 3 turns to avoid abrupt displacements which can potentially damage the machine elements. Therefore, independent power systems of each cavity with a short delay cavity controller are used.[15] A central controller between the two systems across the IP makes the required corrections to adjust the cavity set points as necessary. Figure 12 shows the proposed LLRF architecture.

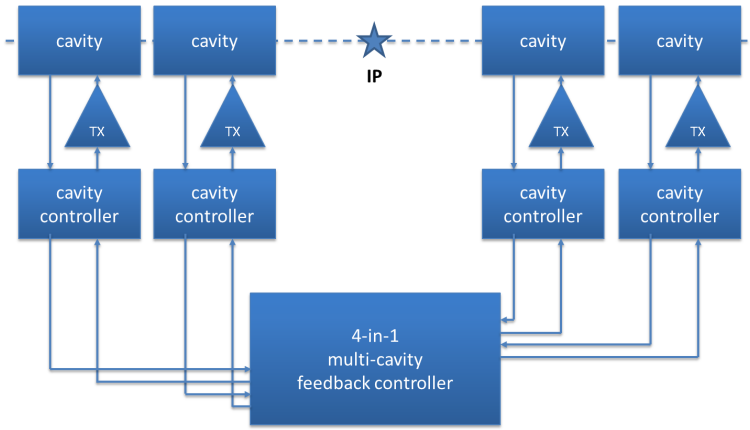

Fig. 12. Proposed LLRF architecture for one ring at one IP for operation with an installation of four cavities per IP per beam.

3.3. *RF Noise and Stability*

Cavity voltage amplitude jitter introduces a residual crossing angle at the IP proportional to the error as shown in Figure 13 (left). It is sufficient that this residual crossing angle is much smaller (< 1%) than the geometric crossing angle leading to required voltage control from electronics:[21]

$$\frac{\Delta V}{V} \ll \frac{1}{\Phi}, \tag{4}$$

where Φ is the Piwinski parameter. A phase error in the RF wave causes an offset of the bunch rotation axis translating into a transverse offset at the IP (cf. Figure 13, right). The offset at the IP is given by

$$\Delta x = \frac{c \cdot \theta_c}{\omega_{RF}} \delta\phi_{RF} \tag{5}$$

where θ_c is the full crossing angle (cf. Figure 13) and ϕ_{RF} is the crab cavity phase w.r.t to the synchronous particle. For the HL-LHC parameters, the voltage error ratio should be kept to below 0.1%. The challenging aspect is to control the phase jitter across the IP to below $5 \cdot 10^{-3}$ degrees to minimize transverse emittance growth. This corresponds to a transverse displacement of 5% of the beam size at the IP.[22]

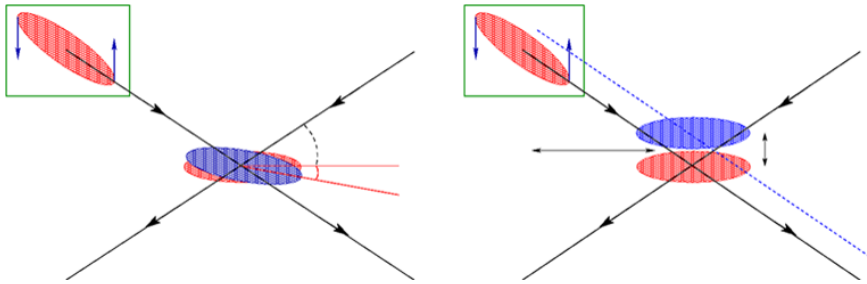

Fig. 13. Schematic of cavity voltage amplitude error leading to a residual crossing angle (left) and a phase error leading to an offset at the IP (right).

The amplitude and phase control must be achieved also during filling and ramping with small (or zero) field in the cavities. Smooth transition between no-crabbing and crabbing must be realized. A single reference generated in a surface building above the accelerating cavities is sent over phase-compensated links to respective crab cavities at IP1 (ATLAS) and IP5 (CMS). An alternative would be to re-generate the bunch phase from local pick-ups.[15]

4. Integration in SPS and LHC

The first proof of principle system with two DQW cavities in a cryomodule was tested in the special SPS test bench in 2018. The primary aim of these tests was to validate the technology with proton beams, demonstrate the ability to make the system transparent and establish a robust operational control of a multi-cavity system for the different modes of operation.

4.1. *SPS Beam Tests*

The SPS ring of a special test region was equipped with a special bypass on a movable table and featuring Y-chambers with mechanical bellows that can be displaced horizontally (see Figure 14). This allowed for the crab module to be placed out of the circulating beam during regular operation of the SPS and to be moved in only during dedicated machine development and not during regular operation. This setup was essential both due to aperture limitations of the crab cavities and the risk associated with leaving the cavities in the beam line with different modes of operation in the SPS.[13]

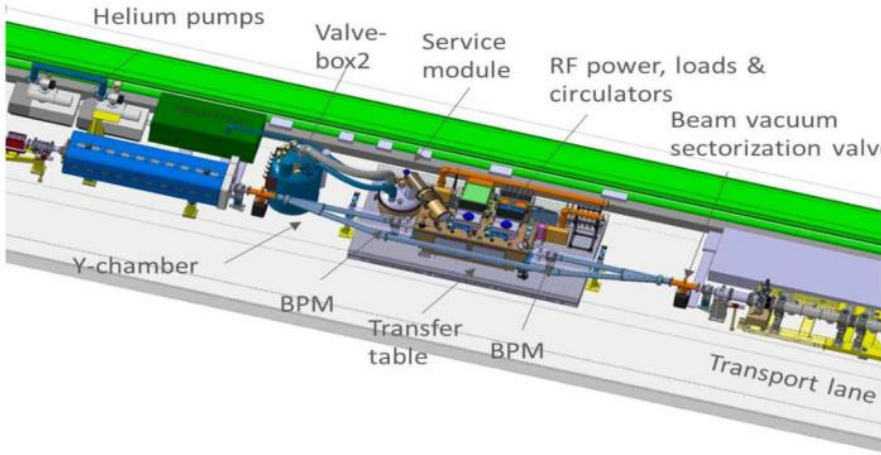

Fig. 14. SPS-LSS6 bypass for the installation of a 2-cavity crab cavity module for the first beam tests with protons.[13]

A complete cryogenic system on the surface (SPS-BA6) and in the tunnel (SPS-LSS6) was installed to deliver 2 K helium for the test operation of the crab cavities. The measured static load of 18 W is almost exactly as the estimated load from design simulations. Two coaxial transmission lines were used to feed RF power of up to 40 kW from the amplifiers (IOTs) installed on the surface. Placement of the passive RF elements (circulators and RF loads) was required to allow for the horizontal movement of the bypass remotely. All beam-pipes in this vacuum sector are coated with a thin film of amorphous carbon, to reduce secondary electron yield and consequently mitigate electron cloud.[14]

A detailed campaign of dedicated experiments were carried out in the SPS with proton beams in 2018. Crabbing of the proton bunches were demonstrated (see Figure 15) for the first time and several aspects related to the RF sychronization, cavity transparency, beam quality preservation and intensity related effects.[25]

4.2. *HL-LHC Integration*

The RF system demands an independent control of each of the 4 cavities per IP side with the shortest delay loops between the RF amplifier and the

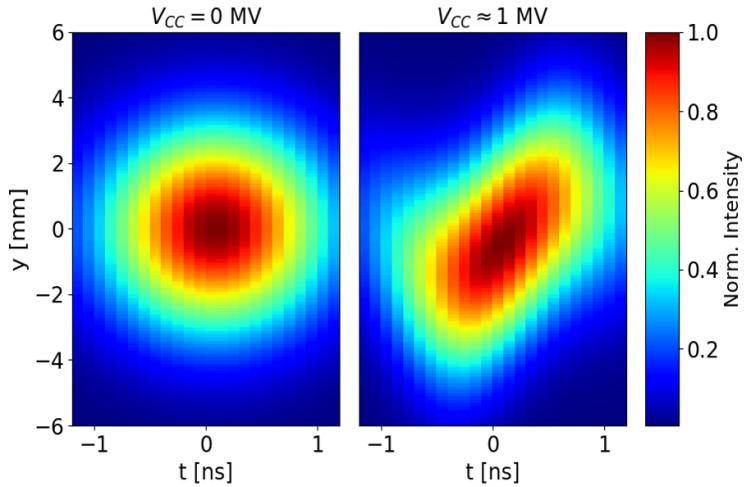

Fig. 15. A comparison of the intra-bunch motion measured with the Head-Tail monitor. The left shows the case where the crab cavities are switched off while the right shows the case where synchronous crabbing is seen with one cavity powered to 1 MV.

cavity (see Figure 12 and Eq. (3)). IOTs provide adequate power overhead in a compact footprint which is presently chosen as the baseline to provide the 40 kW-cw power to each cavity. An IOT based system was successfully operated in during the SPS tests. This scheme would also allow for fast and independent control of the cavity set point voltage and phase to ensure accurate control of the closed orbit and the crossing angle in the multi-cavity scheme. Most importantly, fast control of the cavity fields will minimize the risk to the LHC during an abrupt failure of one of the cavities, ensuring machine protection before the beams can be safely extracted. For such fast and active feedback, a short overall loop delay between the RF system and the cavity is required. A service gallery a few meters above the tunnel (UA galleries) allows for sufficient shielding to sensitive RF electronics and access to the RF equipment during beam operation (see Figure 16). Special cores are placed above the cavities to bring the RF power from the output of the circulators to the cavity to minimize the RF equipment inside the tunnel (see Figure 11). Recent advances in solid-state technology allowed pursuing the study of an SSPA based system in parallel to potentially replace the IOTs and to provide a flexible platform.

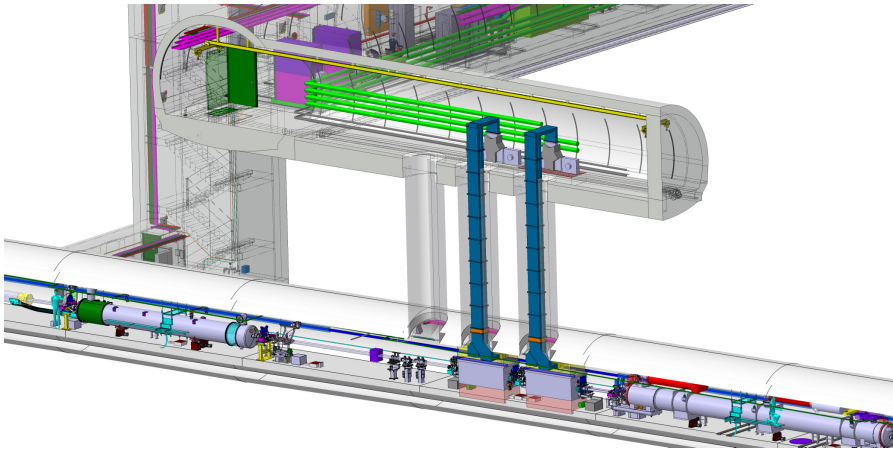

Fig. 16. Preliminary sketch of a high-power RF, controls and LLRF layout in the underground RF cavern.[5]

5. Operational Scenarios

The crab cavities must cope with the various modes of the collider cycle: filling, ramping, and physics.

5.1. *Cavity Transparency*

During filling of the nominally 2748 bunches into the LHC, energy ramping, or operation without crab cavities, the system will be inhibited by making the cavities transparent to the beam (crabbing off). Since more than one cavity is used, counter-phasing to make the effective kick voltage zero while always keeping accurate control of the cavity field is used as the baseline scenario. The counter-phasing ensures both zero effective voltage and beam stability on tune – in fact, it was found that this is the preferred scenario.[15] At flattop, we drive counter-phasing to zero and synchronously change the voltage in all crab cavities as desired. The counter-phasing of two crab cavities was successfully demonstrated in the SPS beam tests in 2018.

Another possibility is to operate with 'crabbing off' while simultaneously detuning the cavity; but a small field and RF feedback should be kept for the required active tuning system. This is referred to as 'parking'. Parking the

cavity half the distance between two revolution frequency side-bands would be ideal for stability. If detuning is used, with a positive non-integer tune ($Q_h = 64.3$, ω_b/ω_{rev} above an integer), the cavity should be tuned above the RF frequency to make the mode $l = -64$ stabilizing (see Figure 17, left).

During a LHC physics run, with crabbing on, the active RF feedback will reduce the peak cavity impedance and transform the high Q resonator to an effective wide-band impedance that covers several revolution frequency lines. The actual cavity tune then has no big importance for stability anymore. Growth rates and damping rates are much reduced, and we have no more dominant mode as shown in Figure 17, right.

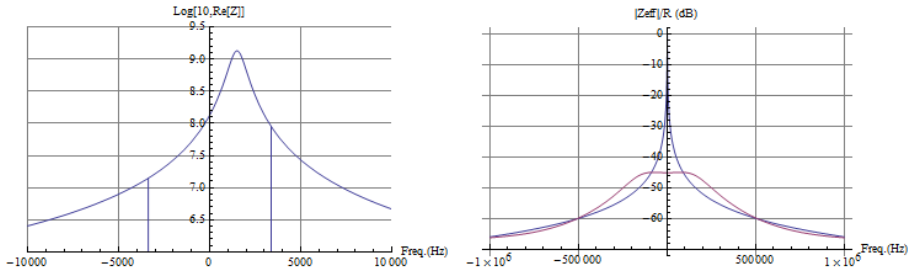

Fig. 17. Left: Real part of the deflecting mode impedance with a detuning of 1.5 kHz from 400 MHz. The vertical lines represent the difference in $Re\{Z\}$ evaluated at $\pm 0.3\ f_{rev}$ for the computation of damping rate (mode $l = -64$). Right: Modulus of the cavity impedance seen by the beam with the RF feedback on (red) and off (blue) normalized to the cavity impedance at the fundamental mode.

5.2. *Injection power Transients*

Injection mismatch at the LHC ring causes beam oscillation along the ring, resulting in beam orbit offsets at the LHC crab cavity. Due to transverse oscillations that can reach up to 2 mm, the power requirement exceeds that available from the 40 kW-CW specification and full compensation of transient beam loading is not possible. A fast transverse damper is used to damp the injections oscillations within 50 turns. Simulations shown that the required crab cavity RF power rapidly converges to the steady state value within 15 turns and should be compatible with the peak power available in the crab cavity RF system.[23]

5.3. *Effects of Full-Detuning*

As explained in subsection 1.1 at the beginning of this chapter, phase modulation of the accelerating cavities is required to minimize the transient beam loading effects (full-detuning). The RF phase of the crab cavities cannot be modulated to follow this phase modulation due to their high loaded quality factors. If the crab cavities are operated from the fixed RF frequency references, it will result in a 60 ps maximum displacement of a bunch centre from the zero phase in the crabbing field. However, the crab cavities are synchronized and for identical bunch phase shifts on the two counter-rotating beams, the bunch centres have the same transverse displacement at the IP. For the longitudinal displacement of the luminous region this may be acceptable given the 1 ns bunch length; the resulting transverse offset of the bunch centroid in the IP however (see above under "RF Noise and Stability") will require that the LLRF synchronizes bunch by bunch correctly taking the actual phase modulation into account. The cumulative effect of this phase shift and the RF curvature was shown in simulations to be negligible.[24]

5.4. *Fast Failures and Machine Protection*

Crab cavity failures can lead to a fast voltage and/or phase change with a short time constant. This can lead to large, global head–tail oscillations, or coherent betatron oscillations with a change in transverse beam trajectories of 1.7σ for a single cavity failure; the effect is cumulative with the number of failing cavities. These failures can be broadly classified into two categories:

- Fast failures, single or few turns. For example, a sudden cavity quench or breakdown.
- Slow failures, several tens of turns or greater (caused by vacuum degradation, voltage and phase drifts, or similar).

Due to the relatively high quality factor in the superconducting cavity, the stored energy inside the cavity can typically only be extracted with a time constant determined by Q_L, which results from the coupling to the cavity via the power coupler. The stored energy will decay with a time constant $\tau = 2 \cdot Q_{L/0}$. For $Q_L = 5 \times 10^5$, the time constant is approximately 400 µs. The three turn delay time (270 µs) for a beam dump trigger is an important consideration during a RF source failure, where the cavity field decays to

roughly half its value before the beam can be safely aborted. In the case of a quench, the time constant of field decay may be dominated by the quench dynamics rather than Q_L. The situation is similar to strong and sudden electron loading due to multipacting or other phenomena.

Two kinds of interlocks are foreseen: slow (on BPMs) and fast (on RF). To minimize the perturbation on the beam during a cavity failure, the MFB will adjust the field in the other cavities on both sides of the IP, such that the orbit distortion due to cavity failure remains local. The rapid change in field will also result in a detuning of the cavity; however, the mechanical tuning system is unable to adjust the tune within 400 μs. Since a rapid breakdown of a failed cavity may become unpredictable, it is probably safest to ramp down the cavities synchronously. However, small and slow changes in one of the cavities can be adjusted for without aborting the beam.

The BPM interlock post-mortem, i.e. the last recorded trajectories could be used to study the effect on beam during a cavity failure. Operationally, it is preferred to have a low Q_{ext} ($\sim 10^5$), as the cavity frequency is less sensitive to perturbations. However, it is assumed that machine protection may benefit from a high Q_{ext} ($\geq 5 \times 10^5$) to help avoid fast reaction on the frequency and phase changes of cavity. Consequently, the cavity will be more sensitive to external perturbations.

References

1. D. Boussard, RF power requirements for a high intensity proton collider, Proceedings of Particle Accelerator Conference (PAC'91) (1991), pp. 2447-2449.
2. P. Baudrenghien, T. Mastoridis, Proposal for an RF roadmap towards ultimate intensity in the LHC, Proceedings of International Particle Accelerator Conference (IPAC'12) (2012), pp. 154-156.
3. T. Mastoridis, P. Baudrenghien, J. Molendijk, Cavity voltage phase modulation to reduce the high-luminosity Large Hadron Collider RF power requirements, Phys. Rev. Accel. Beams, 20 (2017), p. 101003.
4. LHC Design Report, CERN-2004-003-V-3, CERN, 2004.
5. HL-LHC Design Report, CERN-2017-007-M, CERN, 2017.
6. S. Verdu-Andres et al., Design and vertical tests of double-quarter wave cavity prototypes for the high-luminosity LHC crab cavity system, Phys. Rev. Accel. Beams 21, 082002; B. Xiao et al., Design, prototyping, and testing of a compact superconducting double-quarter wave crab cavity, Physical Review Special Topics - Accelerators and Beams 18, 041004. (2015).

7. S. U. De Silva and J. R. Delayen, "Design evolution and properties of superconducting parallel-bar rf-dipole deflecting and crabbing cavities", Phys. Rev. ST Accel. Beams 16, 012004 (2013); S. U. De Silva and J. R. Delayen, "Cryogenic test of a proof-of-principle superconducting rf-dipole deflecting and crabbing cavity", Phys. Rev. ST Accel. Beams 16, 002001 (2013).
8. R. Calaga, "Comments on crab cavity voltage (unpublished)", 2012.
9. W. Hofle, D. Valuch, Transverse Feedback: high intensity operation, AGC, IGC, lessons for 2012, LHC Beam Operation Workshop, Evian, December 2011, CERN-ATS-2012-083, CERN, Geneva (2012), p. 97-100.
10. M. Navarro-Tapia, R. Calaga, A. Grudiev, RF mulipoles from crab cavities, in the proceedings of IPAC13, Shanghai, 2013.
11. J. Barranco et al., Phys. Rev. Accel. Beams 19, 101003 (2016).
12. L. Arnaudon et al., Conceptual specification of the crab cavity RF system, EDMS 1363181, 2014, https://edms.cern.ch/document/1363181.
13. R. Calaga et al., SPS tests of HL-LHC crab cavities, in Proc. IPAC18, Vancouver, 2018.
14. C. Yin Vallgren et al., "Amorphous carbon coatings for mitigation of electron cloud in the CERN SPS", in Proc. IPAC10, Kyoto, Japan, May 2010, pp. 2033–2035.
15. P. Baudrenghien, LLRF for Crab Cavities, presented at the 2nd HiLumi-LHC Meeting, Frascati, 2012.
16. M. Sosin et al., Alignment reference.
17. Dressed cavity citation.
18. K. Artoos et al., Development of SRF cavity tuners for CERN, in the proceedings of the SRF 2015, Whistler, 2015; K. Artoos et al., Status of the HL-LHC crab cavity tuner, in the proceedings of the SRF 2019, Dresden, 2019.
19. T. Capelli et al., in the proceedings SRF 2019, Dresden, 2019.
20. M. Garlasche et al., in the proceedings of the IPAC 2018, Vancouver, 2018.
21. K. Oide, K. Yokoya, Physical Review A, 40, 315 (1989).
22. R. Calaga et al., in the proceeding of the LHC performance workshop 2010, Chamonix, 2010.
23. E. Yamakawa et al., Beam loading study for HL-LHC and measurements in SPS crab cavities, STFC-Report-2018, to be published.
24. E. Yamakawa et al., Luminosity reduction caused by phase modulations at the HL-LHC crab cavities, Nuclear Inst. and Methods in Physics Research, A 908 (2018) 338–346.
25. R. Calaga et al., "First demonstration of the use of crab cavities on hadron beams", Physical review, accelerators and beams 24, 062001 (2021).
26. F. Carra, "DWQCC cryomodule thermal budget and heat loads," EDMS n. 1729079 (2017); J.S Swieszek et al., RFD CC cryomodule thermal budget and heat loads, EDMS n. 2310389, https://edms.cern.ch/document/2310389, (2020).